NUMERICAL STUDY OF A FLAME SPREAD IN RACK STORAGE WITH A BUOYANCY-INDUCED FLOW

P. Russo[1,2], H.Y. Wang[1], P. Joulain[1] and L. Fournier[2]

[1] Laboratoire de Combustion et de Détonique, C.N.R.S. UPR 9028 -E.N.S.M.A., Université de Poitiers BP 109 - Site du Futuroscope, 86960, Futuroscope Cedex, France

[2] Institut National de l'Environnement Industriel et des Risques, Verneuil-en-Halatte, France

(Received 30 May 2006; Accepted 15 September 2006)

ABSTRACT

Large-Eddy-Simulation (LES) is performed to investigate the transport characteristics and structure of large-scale, turbulent fires in rack storage under natural convection conditions. The three-dimensional, time-dependent Navier-Stokes equations are solved with sufficient temporal and spatial resolution. The large-scale eddies are simulated directly and subgrid-scale motion is represented by Smagorinsky model. Combustion process in buoyancy-driven fire plumes is assumed to be diffusion-controlled, permitting a mixture-fraction-based modeling approach. The discrete ordinates method is used for estimating the flame radiation energy to the condensed fuel surface. The numerical models have been validated using experimental data from the turbulent diffusion flames established along the condensed fuel object in rack storage. Based on the validated numerical results, the flame height correlations below and past the rack storage are established. The convective flux plays a dominant mode of heat transfer only for the separation distance between the condensed fuel lower than 75 mm. For the separation distance higher than 75 mm, contribution by radiation is about 80% of the total heat flux. However, unlike a single vertical wall fire, the level of the heat flux at each tier in rack storage does not increase significantly with height, mainly due to the limited view factor in the reacting zone. The conductive heat loss flux in condensed fuel phase is only important in the incipient period of the fire, and can be neglected once the fire is established. A maximum fire growth rate is predicted for a spacing of 150 mm due to the enhanced flame flapping through the buoyancy-induced flow.

1. INTRODUCTION

Flame spread over surface of a condensed fuel in rack storage arrays, as shown in Fig. 1, can be encountered in a warehouse. Such fire in storage arrays is particularly serious due to a naturally induced air flow moving upward along a vertical channel between adjacent stacks (condensed fuel). Up to now, a free vertical wall fire has always occupied a large proportion of the research effort by means of numerical, experimental or empirical methods [1-6]. With the help of the experiment [7] and numerical simulation [8], the fire in storage arrays is simplified as a vertical parallel diffusion flame, and effects of separation distance between the adjacent burning walls are found to be a dominant factor affecting the flames interaction, and consequently the radiation flux and burning rate. The experimental works [9-14] have addressed the fires in rack storage, and some correlations are provided by Heskestad [9-10] and Ingason [14] by taking into account the effects of the rack geometry on the heat release rate, flame height and temperature/velocity fields.

In spite of the important findings [9-14], description of the characteristics of the turbulent diffusion flame, fire-induced draft and in particular, heat transfer in rack storage, is still very limited due to the short experiment duration of gas/solid combustion. In order to understand a turbulent fire propagation in rack storage, this article presents an application of Large-Eddy-Simulation (LES) for solving the fluid dynamic equations of three-dimensional elliptic, reacting flow. Fire Dynamics Simulator (FDS), developed by NIST [15], appears more advantageous in the computational cost for such fire with a buoyancy-induced draft. The fire itself is prescribed in a manner consistent with mixing-controlled combustion, permitting a mixture-fraction-based modeling approach. The present work uses finite-difference method to discretize the appropriate conservation equations. The radiative transfer equation is solved through the discrete ordinates method [16] for calculating the radiative heat flux which is responsible for a large fraction of the energy transferred to the burning surface. The total absorption coefficient of the mixture of CO_2, H_2O, and soot particles is incorporated into the radiation model. This approach to the field modeling of fire phenomena emphasizes high enough spatial and temporal resolution with an efficient flow solving technique. Predictions of the flame structure and buoyancy-induced flow are compared with the available

transient measurements [14] in rack storage arrays, and good agreement is found.

Fig. 1: Release examined experimentally by Ingason

2. THEORETICAL ANALYSIS

The motion of the fluid induced by buoyancy is governed by the equations written in a form suitable for Low Mach number applications [15]. In simulating these flows, the acoustic modes can be removed from the governing equations, resulting in significant computational savings. In the following sections, brief descriptions are presented of the turbulence, combustion and radiation models, and of the solving procedure.

2.1 Fluid Dynamics

In LES, the filtering operation decomposes a full field, $\phi(x,t)$, into a resolved component $\bar{\phi}(x,t)$ and a subgrid-scale component $\phi'(x,t)$ [15]. Applying the filtering operation to each term in the conservation equations of mass, momentum, energy and species, and decomposing the dependent variables (u, v, w, p, etc.) into resolved and subgrid components results in the filtered governing equations, shown below:

$$\frac{\partial \rho}{\partial t} + \frac{\partial \rho \bar{u}_j}{\partial x_j} = 0 \qquad (1)$$

$$\frac{\partial \rho \bar{u}_i}{\partial t} + \frac{\partial (\rho \bar{u}_i \bar{u}_j)}{\partial x_j} + \frac{\partial \bar{p}}{\partial x_i} - \rho g_i = \nabla \cdot \bar{\tau}_{ij,SGS} \qquad (2)$$

where an overbar denotes the filtered variable. The large-scale eddies that govern the mixing of the gases are directly computed at the resolved scale. The scales of motion unresolvable on the computational mesh are modeled by using the Smagorinsky model [15] which relates the unknown Sub-Grid Scale (SGS) Reynolds stresses, $\bar{\tau}_{ij,SGS}$, to the local large scale rate of strain.

$$\bar{\tau}_{ij,SGS} - \frac{1}{3}\bar{\tau}_{kk,SGS}\delta_{ij} = 2\mu_t \bar{S}_{ij} \qquad (3)$$

where

$$\bar{S}_{ij} = \frac{1}{2}\left(\frac{\partial \bar{u}_i}{\partial x_j} + \frac{\partial \bar{u}_j}{\partial x_i}\right) \text{ and } \mu_t = C_s^2 \rho \Delta^2 \left|\bar{S}_{ij}\right| \qquad (4)$$

Here, $\left|\bar{S}_{ij}\right|$ is the magnitude of the large scale strain rate tensor $\bar{S}_{ij}$, and Δ is the filter width, defined as:

$$\Delta = \left(\Delta x \Delta y \Delta z\right)^{1/3} \qquad (5)$$

The filter width, Δ, represents the smallest scale of the resolved field, and is directly related to the grid spacing of the LES computational mesh. The length scale of viscosity, μ_t, is tied to the grid used in the calculations, and its time scale is determined by the local resolvable dissipation. The standard value of the Smagorinsky constant, C_s, is assigned to 0.21.

The SGS motions are based on an eddy viscosity concept, resulting in the filtered energy equation:

$$\frac{\partial \rho \bar{h}}{\partial t} + \frac{\partial (\rho \bar{u}_j \bar{h})}{\partial x_j} = \frac{\partial}{\partial x_j}\left(\frac{\mu_t}{Pr_t}\frac{\partial \bar{h}}{\partial x_j}\right) + \dot{q}_c + q_r \qquad (6)$$

Here, Pr_t denotes the turbulent Prandtl number, chosen as 0.5. Finally, the perfect gas law is used to describe the equation of state:

$$p_0 = R\rho\bar{T}\sum_i \frac{\bar{Y}_i}{W_i} \qquad (7)$$

2.2 Combustion Model

In this study, the reaction kinetics of the condensed fuel (carton) is considered as those of wood ($C_{3.4}H_{6.2}O_{2.5}$). A global one-step irreversible chemical reaction for complete combustion is assumed. With the infinitely fast-chemistry assumption of Schvab-Zeldovich formulation, the combustion processes are governed by the conservation equation for the filtered mixture fraction, $\bar{f}$, written as:

$$\frac{\partial \rho \bar{f}}{\partial t} + \frac{\partial (\rho \bar{u}_j \bar{f})}{\partial x_j} = \frac{\partial}{\partial x_j}\left(\frac{\mu_t}{Sc_t} \frac{\partial \bar{f}}{\partial x_j} \right) \quad (8)$$

where Sc_t denotes the turbulent Schmidt number, given as 0.5. The oxygen mass conservation equation is given as:

$$\frac{\partial \rho \bar{Y}_o}{\partial t} + \frac{\partial (\rho \bar{u}_j \bar{Y}_o)}{\partial x_j} = \frac{\partial}{\partial x_j}\left(\frac{\mu_t}{Sc_t} \frac{\partial \bar{Y}_o}{\partial x_j} \right) + \dot{\omega}_o \quad (9)$$

For the thin flame sheet model, the state relations between the mass fraction of each specie and mixture fraction can be established. Equation (9) can be transformed into an expression for the local oxygen mass consumption using the conservation equation (8) for the mixture fraction and state relation for oxygen $Y_o(f)$ [15].

$$-\dot{\omega}_o = \frac{\partial}{\partial x_j}\left(\frac{\mu_t}{Sc_t} \frac{dY_o(f)}{df} \frac{\partial f}{\partial x_j} \right) - \frac{dY_o(f)}{df} \frac{\partial}{\partial x_j}\left(\frac{\mu_t}{Sc_t} \frac{\partial f}{\partial x_j} \right) \quad (10)$$

The heat release rate is directly proportional to the rate of consumption of oxygen:

$$\dot{q}_c = -H_o \dot{\omega}_o \quad (11)$$

Here, H_o is the heat release rate per unit mass of oxygen consumed.

2.3 Radiation Model

The source term of the energy equation (6) is also a function of the radiant flux vector. It is calculated by integrating the radiation intensity over all directions and wavelengths. The radiation intensity is found by solving the following Radiative Transfer Equation (RTE) without scattering as the soot particles are small:

$$\vec{\nabla}.\vec{\Omega} I + \kappa I = \kappa \frac{\sigma T^4}{\pi} \quad (12)$$

Here, the RTE (12) includes a balance of radiant energy emitted into the direction of propagation and radiant energy attenuation due to absorption by the medium.

The RTE (12) describing the spatial variation of radiative intensity, I, along each direction, is solved through the use of a Finite Volume Method [16]. A discrete equation for a single ordinate direction l, which is derived from the RTE (12) by substituting a quadrature summed over each ordinate direction into the integral term, can be written as:

$$\sum_{m=1}^{6} A_m I_m^l (\Omega^l \cdot \mathbf{n}_m) \delta\Omega^l = \kappa \left[\frac{\sigma T^4}{\pi} - I^l \right] V \delta\Omega^l \quad (13)$$

where A_m is the area of cell face m, and V cell volume. Finally, the radiative source term, q_r, in the energy equation (6) is calculated from the divergence of the radiative flux, given as:

$$q_r = -\int_{4\pi} \vec{\nabla}.\vec{\Omega} I \, d\Omega \approx \kappa \left(\sum_{l=1}^{N} w^l I^l(r) - 4\sigma T^4(r) \right) \quad (14)$$

The total absorption coefficient, κ, of the combustion products is calculated from the code RADCAL [15] for the mixture of CO_2, H_2O and soot particles ($Y_{soot} = 0.01$).

2.4 Pyrolysis Model

A one-dimensional heat conduction is applied in the normal direction, n, of the condensed phase,

$$\frac{\partial T_s}{\partial t} = \alpha_s \frac{\partial^2 T_s}{\partial n^2} \quad (15)$$

The boundary condition over a condensed fuel surface is:

$$-k_s \frac{\partial T_s}{\partial n}(0) = \dot{q}_{conv} + \dot{q}_{rad} - \dot{q}_{pyro} \quad (16)$$

Here, $\dot{q}_{pyro}$ is energy available for pyrolyzing fuel. The thermal diffusivity, α_s, of 1.1 x 10^{-7} and conductivity, k_s, of 0.1 ($Wm^{-1}K^{-1}$) are chosen for the paper carton. Flame radiation flux, $\dot{q}_{rad}$, is computed from a discrete representation of the radiative intensity equation (13). Conditions similar to those of an equilibrium turbulent boundary layer (Couette flow) are assumed to prevail, and the convective heat feedback is determined from the local thermodynamic properties and velocity [15]. The mass loss rate, $\dot{m}_s$, of volatiles from the surface of the condensed fuel is assumed to obey the simple Arrhenius expression:

$$\dot{m}_s = A e^{-E/RT} \ (kgm^{-2}s^{-1}) \quad (17)$$

Here, the frequency factor, A, of 2.6 x 10^8 and activation energy, E/R, of 12000 are used for this paper carton.

2.5 Method of Resolution

In order to complete the mathematical description, the boundary conditions should be specified. The no-slip condition is imposed by setting all velocities to zero at the solid surface. The burning wall is considered as a pure combustible material

($\bar{f}_w$ = 1). However, the mixture fraction at the burning surface ($\bar{f}_s$ < 1) is adjusted during the numerical iteration, according to the following conservation relationship:

$$(1-\bar{f}_s)\dot{m}_s = -\frac{\mu_t}{Sc_t}\frac{d\bar{f}_s}{dn} - \Delta t u_s \frac{d(\dot{m}_s \bar{f}_s)}{dn} \qquad (18)$$

Here, Δt is the time step, u_s the fuel injection velocity (ms^{-1}), and $\dot{m}_s$ fuel surface injection rate ($kgm^{-2}s^{-1}$) through the burning wall. At the free boundaries, the perturbation pressure is assumed zero. Zero gradient conditions are used for the free boundary values of the mass fractions. The finite-difference technique is used to discretize the partial differential equations and the associated boundary condition. This procedure entails the subdividing of the calculation domain into a finite number of cells. The velocities (u, v, w) are taken on the boundary of each cell; and all the scalar variables are taken at cell centers. This staggered grid leads to a very efficient differencing scheme for the equations. All spatial derivatives are approximated by second-order central differences and the flow variables are updated in time using an explicit second-order Runge-Kutta scheme. The pressure is found by applying the divergence-free condition to the momentum equations, which yields a Poisson equation which is solved by an efficient direct solver [15].

3. RESULTS AND DISCUSSION

At first, validation of the LES code [15] against detailed experimental data from a buoyancy driven fire in rack storage is performed. The schematic diagram of the release, examined experimentally by Ingason [14], is shown in Fig. 1, and the coordinate system adapted in numerical simulation is presented in Fig. 2. The rack storage consists of four tiers with a total height of H = 5.2 m. Four cartons with the dimensions of 1.2(x) × 0.8(y) × 1.0(z) m^3 were symmetrically placed at each tier. As the experiment, four ignition sources, each with a heat release of 30 kW during 30 seconds, were placed close to the centre of the storage arrays at the bottom of each carton of the first tier. In the experiment, the temperatures were obtained by means of fine wire analogue compensated thermocouples, and the velocities were determined using the bi-directional pressure probes. A higher density of grid nodes is generated using a series distribution close to the wall, and a uniform grid spacing is used in the vertical direction. No significant difference of the predicted results with different grid systems is observed. It was found that the mildly stretched grid system, 48 (x) x 48 (y) x 250 (z), offered the best tradeoff between accuracy and cost. A calculation required about 15 x 24 h on HP4000 workstation for 4 minutes simulation of the events. As Ingason's experiment [14], a range of the horizontal separation distance, w, between the cartons varying from 75, 100, 150 up to 300 mm is considered.

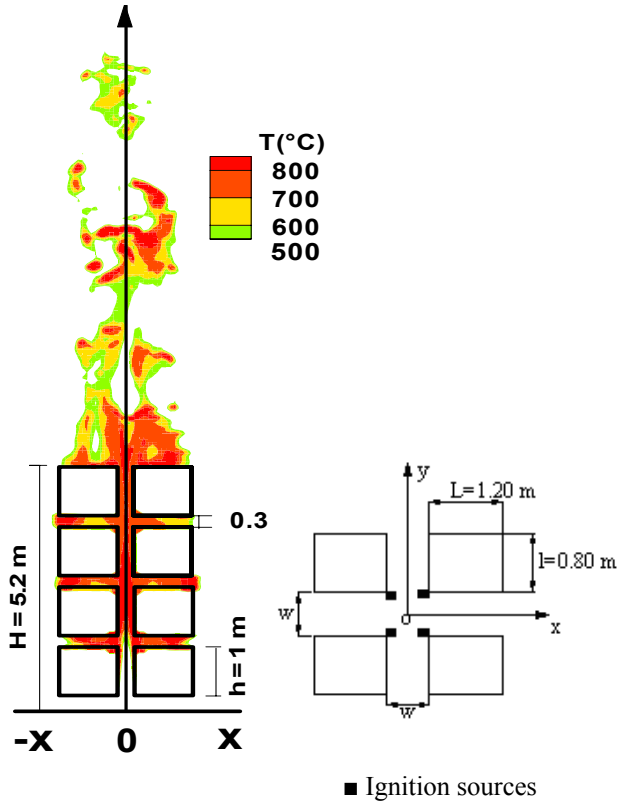

Fig. 2: Schematic diagram of the experimental release and the coordinate system adapted in numerical simulation

After the ignition at the base of the rack storage, the high temperature gases heat the surface of the condensed fuel downstream through convection and radiation. The plume of hot, burning or post-combustion gases can reach the flammable, initially inert stack, and starts heating its surface by radiation and convection up to its pyrolysis temperature. The surface of the condensed fuel will pyrolyze around the ignition temperature of 250 °C, providing the fuel vapor for combustion. The fire development is characterized by a combination of the exponential and power law variations with the following expression:

$$Q_c = H\alpha\, e^{\beta t}(a+bt) \qquad (19)$$

The parameters α,β,a,b can be determined from experimental data or prediction. Comparison between the experimentally-determined [14] and predicted Heat Release Rate (HRR) as a function of time for the different spacing, w, is shown in Figs.

3a and b. Globally, the dependence of the slope of the predicted HRR curves to the spacing, w, follows closely the measured trend. It should be noted that in the numerical simulation, the rack storage is considered as a condensed fuel object with a density of $\rho_s = 23.65$ kgm^{-3}; decrease of the predicted HRR during the fire is due to the progressive consumption of the condensed fuel. It seems that the predicted incipient period is shorter as compared to the measured one, mainly due to the simplified pyrolysis model. During the fire growth period, the slope of the curve of the HRR increases with the spacing, w. In both the prediction and experiment, the spacing of 150 mm gives the shortest incipient and take-off periods of the fire, leading to the most hazardous fire spread.

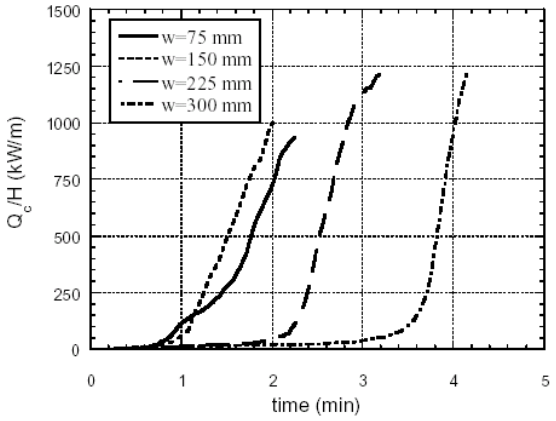

(a) Experiment

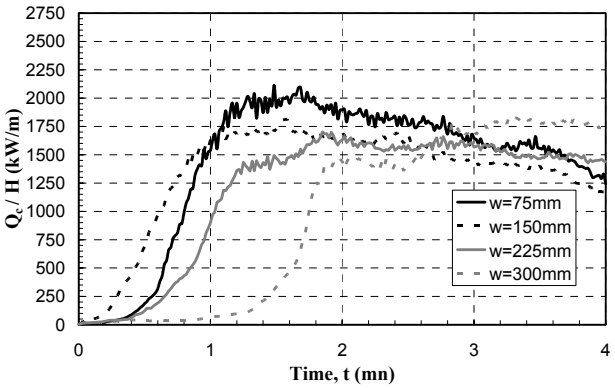

(b) Prediction

Fig. 3: Comparison between the experimentally-determined and predicted HRR as a function of time for the different spacing, w

The time-averages of the instantaneous temperature output on the middle plane (x,z) generate a diffusion flame as a function of the heat release. Below the rack ($z \le H$), the Ingason's experimental data [14] suggests a flame height correlation during the fire spread as follows:

$$L_f = -3.73\, w + 0.343 Q^{2/5} \quad (20)$$

For the prediction, the isothermal contours for the temperature higher than 500°C corresponding to a luminous yellow sooty flame in the experiment, are considered as the visible flame shape. A comparison between the prediction and Ingason's correlation for the flame height as a function of $Q^{2/5}$, is plotted in Fig. 4 for different horizontal spacing, w. It can be seen that for $Q^{2/5}/w < 50$ (kW$^{2/5}$/m), the predicted flame height as a function of the heat release rate, $Q^{2/5}$, follows closely the Ingason's correlation (20) trend. However, for $Q^{2/5}/w > 50$ (kW$^{2/5}$/m), the prediction moves away considereably the Ingason correlation (20). Based on the criterion of 500 °C for the flame height, the numerical results suggest an analytical relation below the rack as follows:

$$L_f = -9.0125w + 0.5004 Q^{2/5} \quad (21)$$

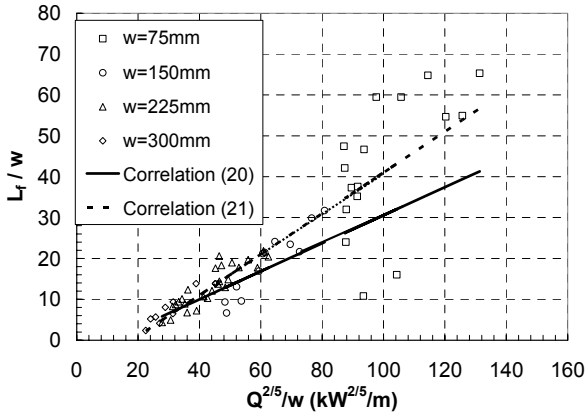

Fig. 4: Comparison between the prediction and Ingason's correlation for the flame height as a function of $Q^{2/5}$ for different spacing, w

From the correlations (20-21), it can be seen that the flame spread height increases with a reduction in the separation distance due to an increase of the buoyancy effects. Past the rack top ($z > H$), the fire seems a turbulent jet flame. A correlation has been developed by Delichatsios [17] for a circular turbulent jet fire. Comparison between the prediction and Delichatsios's correlation for the turbulent jet flames as a function of $\dot{Q}^*$ is presented in Fig. 5.

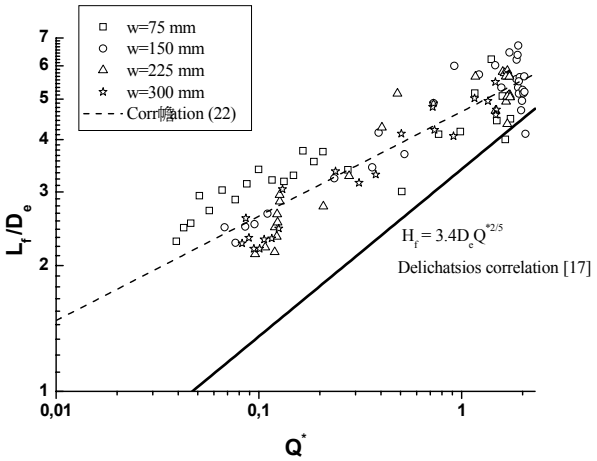

Fig. 5: Comparison between the prediction and Delichatsios's correlation for the turbulent jet flames as a function of $\dot{Q}^*$

It is found that the Delichatsios's correlation is not suitable for the rack storage fire. Based on the predicted temperature field, the Delichatsios's correlation [17] is adjusted for calculating the flame height past the rack top as a function of the HRR, $\dot{Q}^*$, as follows:

$$L_f = 4.67 D_e \dot{Q}^{*\,1/4} \qquad (22)$$

In the correlation, an equivalent diameter, D_e, determined from the fire surface above the rack storage, is used:

$$D_e = 2\sqrt{\frac{(2L+w)\cdot(2l+w)}{\pi}} \qquad (23)$$

A comparison between the predicted and measured temperature, ΔT, along the in-rack excess centreline as a function of the convective heat release rate is plotted in Figs. 6a and b. The symbols represent the measured results in Fig. 6a or prediction in Fig. 6b, and the lines the correlation established by Ingason [14], as follows:

$$\Delta T = 28\left[\frac{T_\infty}{g c_p^{\,2} \rho_\infty^{\,2}}\right]^{1/3} \frac{Q_c^{\,2/3}}{(z-z_0)^{5/3}} \qquad (24)$$

where z_0 is the virtual source location, defined as:

$$z_0 = -3.73w + 0.0083 Q^{2/5} \qquad (25)$$

It can be seen that the predicted temperature increases with HRR to a maximum during the fire growth period in which $(z\text{-}z_0)/Q_c^{2/5}$ is higher than 0.2 m/kW$^{2/5}$, following the power -5/3 of the abscissa. As the fire is established along the rack storage, the temperature remains almost constant, and an increase of the separation distance between the condensed fuels from 75 to 300 mm induces a significant decreases of the temperature from 1000 to 800 °C in the core flow region. Also, an analytical relation of the vertical gas velocity, w, along the rack centreline is established [14] as a function of the convective heat release rate.

$$u_z = 3.54\left[\frac{g}{c_p \rho_\infty T_\infty}\right]^{\frac{1}{3}} \left(\frac{Q_c}{z-z_0}\right)^{0.45} \qquad (26)$$

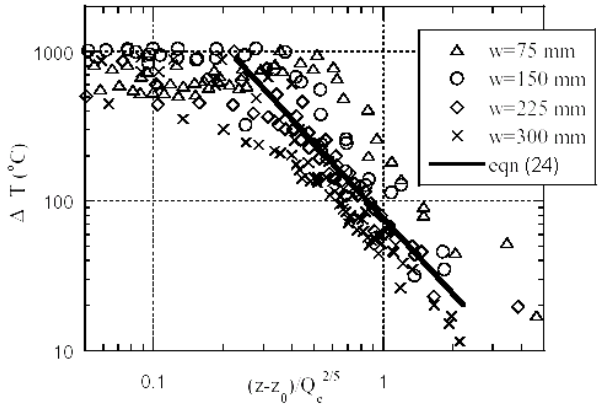

(a) Experiment

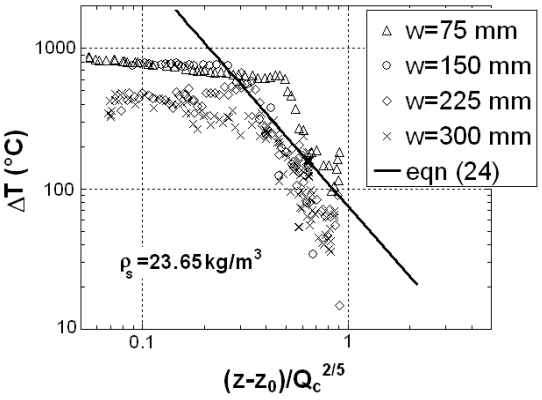

(b) Prediction

Fig. 6: Comparison between the predicted and measured temperature, ΔT, along the in-rack excess centreline as a function of the convective heat release rate

A comparison between the predicted and measured gas velocity along the rack centreline as a function of the convective heat release rate is presented in Figs. 7a and b. As the experimental trend, the predicted velocity increases with HRR to a maximum during the fire growth period in which $Q_c^{1/3}/(z\text{-}z_0)^{1/3}$ is lower than 5 kW$^{1/3}$/m$^{1/3}$. As the fire is established along the rack storage, the vertical

velocity remains almost constant, and a reduction in the separation distance from 300 to 75 mm leads to an increases of the vertical velocity from 9 to 12 ms^{-1} in the core flow region. In general, a good agreement between the prediction and measurement or correlation [14] is observed in terms of magnitude and distribution. This means that the transient characteristics of the fire spread in rack storage are correctly predicted. During the fire growth period, as compared to the measurements, an over-estimation of 10% is found mainly due to the use of a simple one-step chemical reaction model. Another possible source of error is the measurements due to the buoyant instability, yielding the measured values with an uncertainty of 10 to 15%.

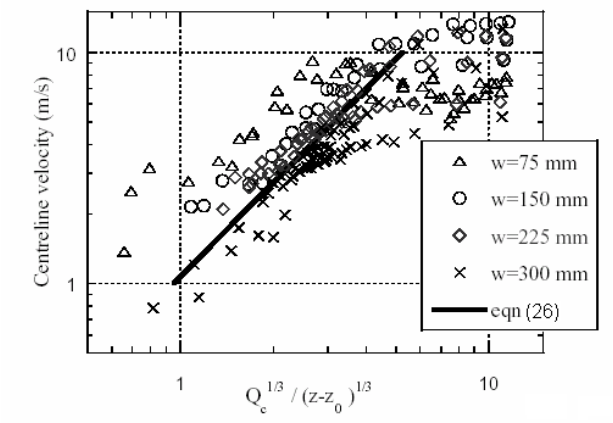

(a) Experiment

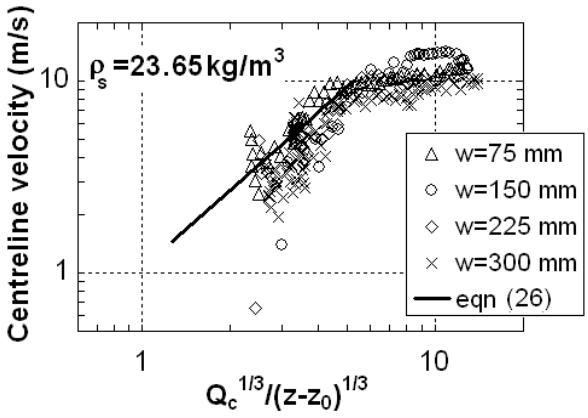

(b) Prediction

Fig. 7: Comparison between the predicted and measured gas velocity along the rack centreline as a function of the convective heat release rate

The transversal profiles of the temperature and vertical velocity in the median plane for the 4 separation distances at different heights are presented in Figs. 8a to d and 9a to d. Three characteristic temperature and velocity features are identified as a function of the separation distance considered here.

1) For the separation distance of w = 75 mm, a rapid increase of the temperature in the centre region is observed with height, z, due to merging of the diffusion flames occurring at a height of 2.5 m. The off-peak temperature forming at low base of the rack persists all along the rack due to the insufficient air entrainment in the narrow spacing for maintaining the combustion. Corresponding to the temperature distribution, an off-peak velocity is also formed at low base of the rack. However, the flow can be strongly accelerated through the combined effects of natural convection and air entrainment, the off-peak velocity disappears just past the rack top.

2) However, when the separation distance becomes sufficiently great (w = 300 mm), the diffusion flames are completely separated all along the rack, characterized by an off-peak in both the temperature and velocity distributions in the centre region.

3) A complex reacting flow structure is established due to the transient flame structure between merging and separation for a moderate separation distance (w = 150 – 225 mm). An off-peak temperature is first formed at the low base of the rack, and replaced later by a peak one due to the merging of the diffusion flames at a height of 4 m. The maximum temperature is always located near the burning surfaces. The off-peak velocity is also formed at the low base of the rack, and a peak velocity (Figs. 9b and c) occurs in the center region once the diffusion flames meet each other.

For the vertical rack fire, the local Grashof number with height (z) can be formulated as:

$$Gr_z = \frac{g z^3}{\nu_0^2} \qquad \text{with } \nu_0 = 15 \times 10^{-6}\ m^2 s^{-1} \qquad (27)$$

With respect to the horizontal separation distance, w, the Reynolds number, Re, of the buoyancy-induced flow is defined as:

$$Re = u_z w / \nu_0 \qquad (28)$$

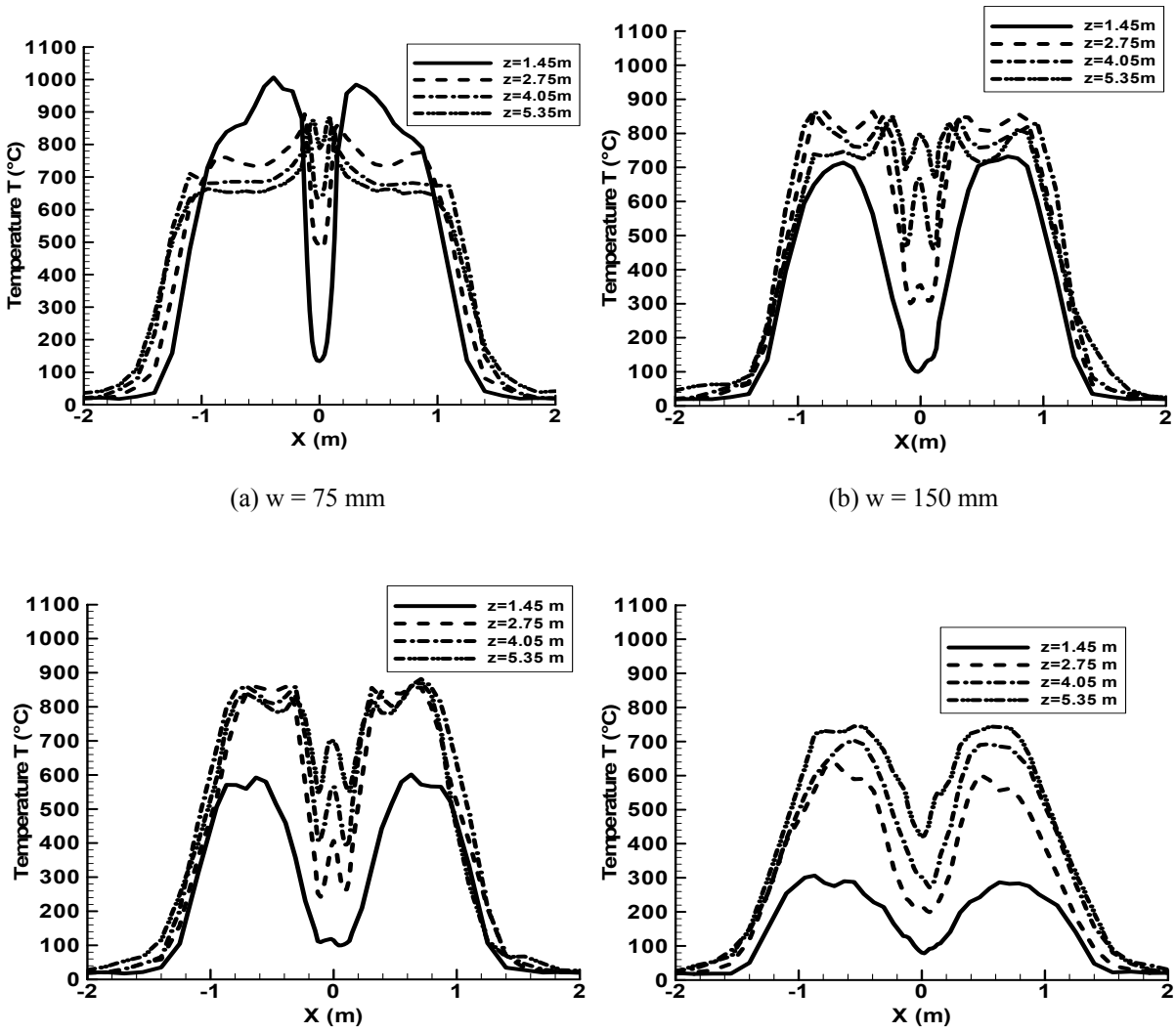

Fig. 8: Transversal profiles of the temperature in the median plane at different heights

For the separation distance, w, varying from 75 to 300 mm, the minimum ratio of Gr_z / Re^2 is higher than 20. In this case, the flow is solely induced and vertically accelerated by buoyancy forces, leading to a constant adimensional vertical velocity, $U^*_{z,max}$, defined as:

$$U^*_{z,max} = \frac{U_{z,max} z}{\nu_0} Gr_z^{-1/2} \quad (29)$$

It is found that equation (29) correlates quite well the predicted velocity field in the median plane, with the approximate constant value of the adimensional velocity, $U^*_{z,max} \approx 6.5$, far away from the base of the rack storage ($z-h_0 > 1$). Following this approach, the maximum axial velocity, $U_{z,max}$, can be written solely as a function of the rack height:

$$U_{z,max} \approx 6.5\sqrt{z - h_0} \ (ms^{-1}) \quad (30)$$

where h_0 is the vertical distance between the first tier base and ground level.

Profiles of the time-averaged longitudinal velocity fluctuation, u', and temperature one, T', in the median plane just past the rack top (y = 0, z/H = 1) are presented in Figs. 10a and b. The temperature fluctuation first increases as the spacing increases from 75 to 150 mm, and later remains practically constant in the core flow region for the further increase of the spacing. For the buoyancy induced flow, the reacting flowfield is displaced in a strong flapping manner, resulting in an increase of the velocity fluctuation due to the enhanced buoyancy

effects as the spacing, w decreases. The higher velocity and temperature fluctuations occur near the air entrainment layer where the strong temperature and velocity gradients induce the large-scale coherent structures.

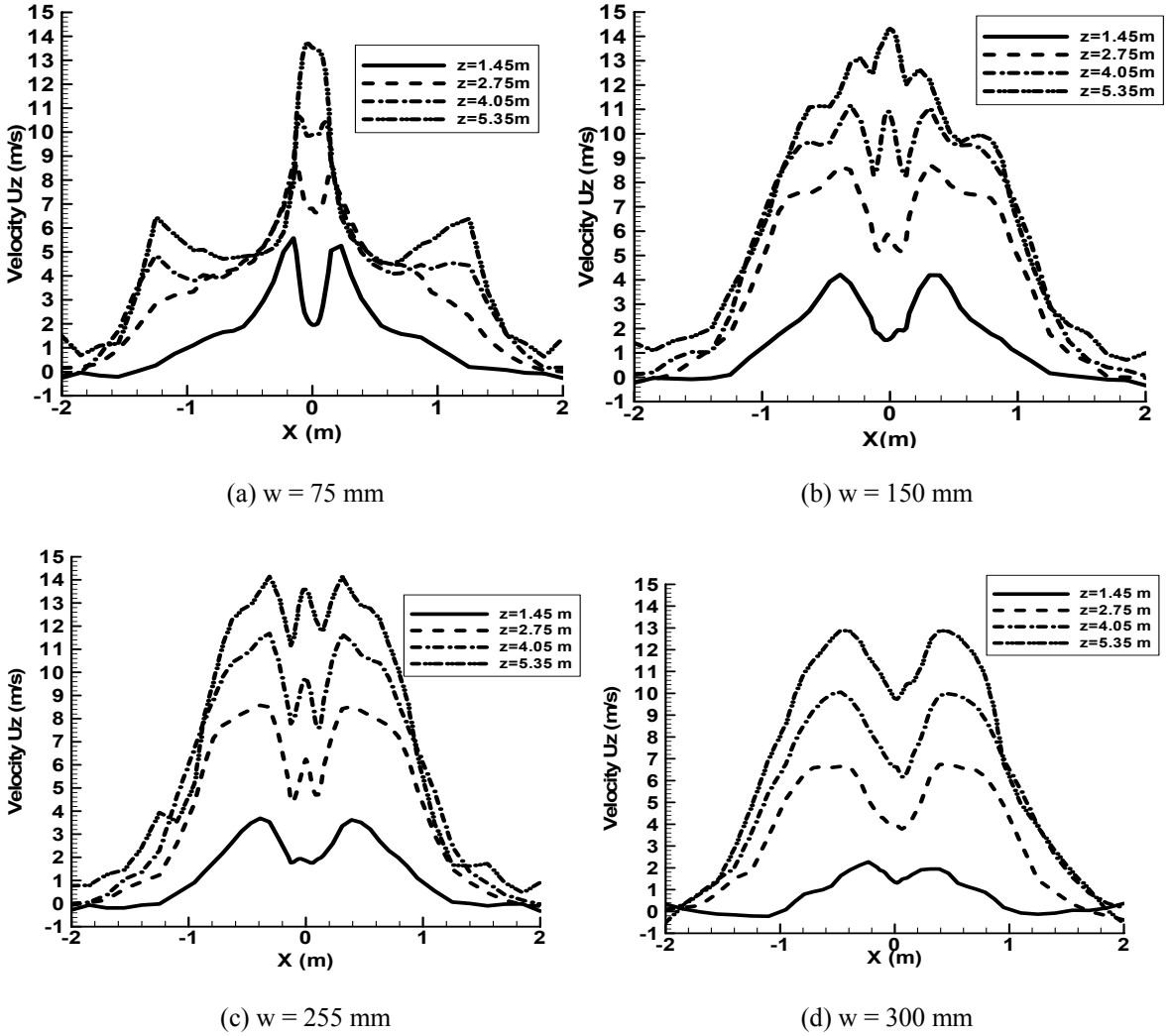

(a) w = 75 mm

(b) w = 150 mm

(c) w = 255 mm

(d) w = 300 mm

Fig. 9: Transversal profiles of the vertical velocity in the median plane at different heights

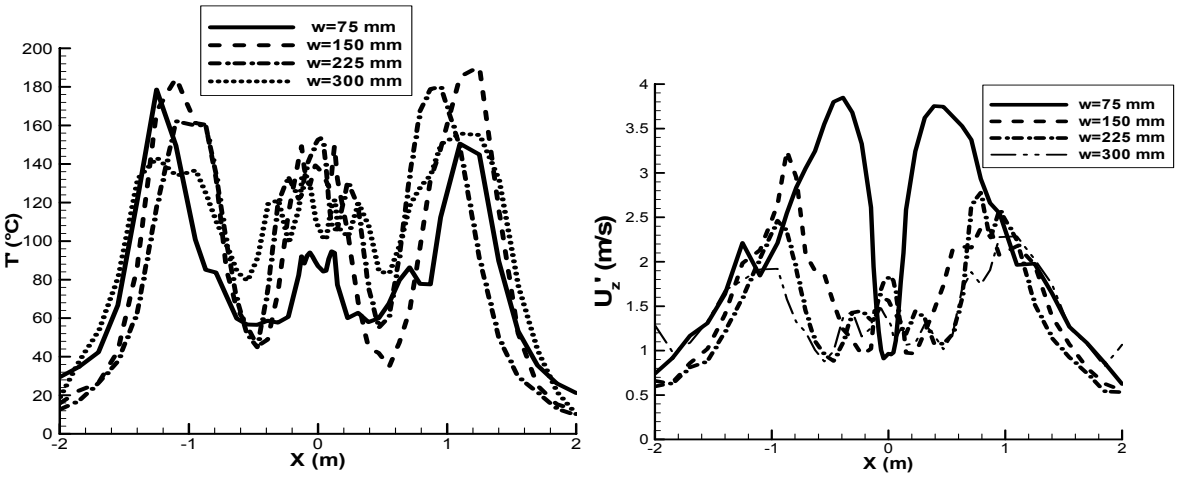

(a) Temperature fluctuations, T'

(b) Longitudinal velocity, u'

Fig. 10: Profiles of the time-averaged turbulent quantities in the median plane just past the rack top

In order to assess the effects of the separation distance on the heat transfer mechanisms, the heat flux is analysed along a vertical line near the fire, as indicated in Fig. 11. Evolution of the convective flux, $\dot{q}_{conv}$, radiative flux, $\dot{q}_{rad}$, and conduction loss in condensed phase, $\dot{q}_{cond}$, are presented in Figs. 12, 13 and 14a to c for the three characteristic steps during the fire development. The first step corresponds to an incipient period of the fire with a HRR of about 250 kW, the second to the fast fire growth period with a HRR of about 1000 kW and the last the established fire over the rack. Three characteristic heat transfer features are identified as a function of the separation distance.

1) At the first step, around the last tier, the convective flux (Fig. 12a) is almost insensitive to the separation distance with a maximum of 5 kWm^{-2}. However, the radiation flux (Fig. 13a) as a whole is proportional to the radiation view factor associated with the separation distance, thus improving the radiation flux for an increase of the separation distance. For the separation distance below 225 mm, the conduction loss (Fig. 14a) in the condensed fuel phase remains almost constant with 5 kWm^{-2}. However, for the separation distance of w = 300 mm, a rapid heating of the condensed fuel surface due to the stronger radiation flux (Fig. 13a) induces a locally pronounced temperature gradient, resulting in a significant conduction loss flux up to 40 kWm^{-2} (Fig. 14a).

2) During the second period, the fire growth induces a large distribution of the high convection flux (Fig. 12b), and its maximum increases from 5 to 10 kWm^{-2} due to turbulence development of the buoyancy-controlled flow. For the separation distance below 300 mm, the maximum of the conduction heat loss flux (Fig. 14b) in the condensed fuel phase increase from 10 to 15 kWm^{-2}. However, for w = 300 mm, a weak conduction loss flux (Fig. 14b) has been established in the condensed phase due to a decrease of the temperature gradient. The flame radiation flux (Fig. 13b) is found to monotonously increase with the separation distance.

3) As the fire is established over the rack, a dramatic reduction in the convection flux (Fig. 13c) at the base of the rack storage (first tier) is brought about as the separation distance increases to 300 mm. For w < 300 mm, the convection flux (Fig. 13c) progressively decreases with height from a maximum in the leading edge zone due to an increase of the flame stand-off distance. The conductive loss flux (Fig. 14c) along the condensed fuel surface becomes independent to the separation distance with a weak value of 4 kWm^{-2}. At the base of the rack storage (first tier), the radiation flux (Fig. 13c) increases first with increase of the separation distance from 75 to 225 mm, and later, significantly decreases for a further increase of the spacing to 300 mm due to flame extinction there. Starting from the second tier, the radiation flux (Fig. 13c) significantly increases with increase of the separation distance, w, from 75 to 225 mm due to an increase of view factor in the reacting zone, and approaches asymptotically that of w = 300 mm. Moreover, unlike a single vertical free wall fire, the level of the heat flux at each tier in rack storage does not increase significantly with height, mainly due to the limited view factor in the reacting zone.

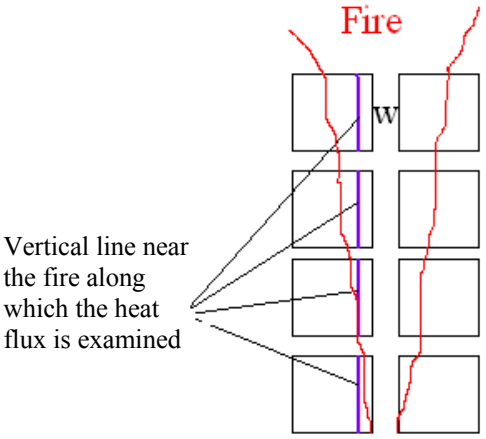

Fig. 11: Characteristic vertical line near the fire over which the heat flux is examined

It seems that the contribution by radiation is a strongly depending parameter on both the separation distance and fire growth step. Globally, the contribution by radiation is higher than 80% of the total heat flux for the larger separation distance (w > 75 mm). Starting from the second tier, changes in the heat fluxes at walls in rack storage are induced by a change in the dominant heat flux mechanism from radiative to convective as the separation distance is reduced to 75 mm. The conduction heat loss flux in condensed fuel (paper carton) phase is only important in the incipient period of the fire, and can be neglected as the fire is established.

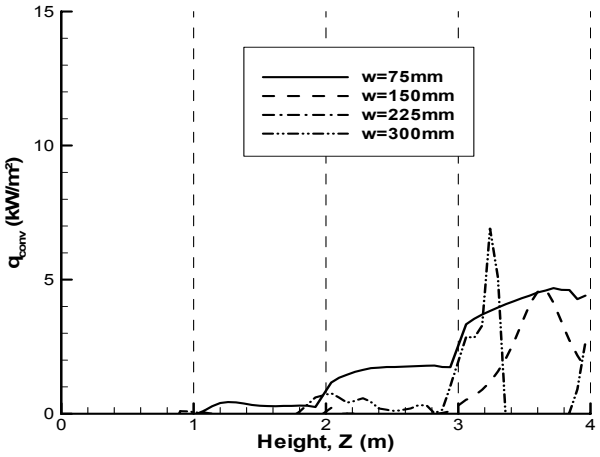

(a) Incipient period

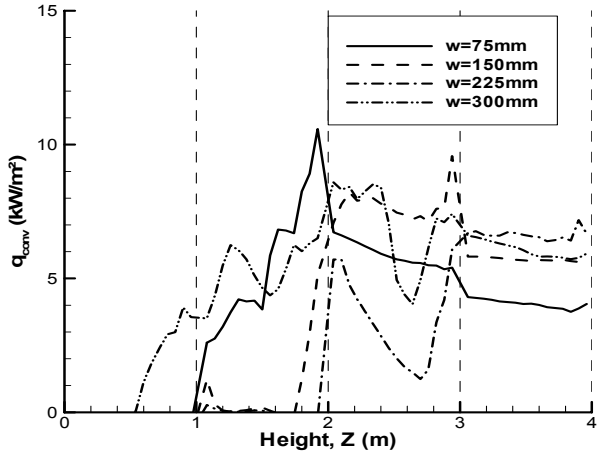

(b) Fire growth period

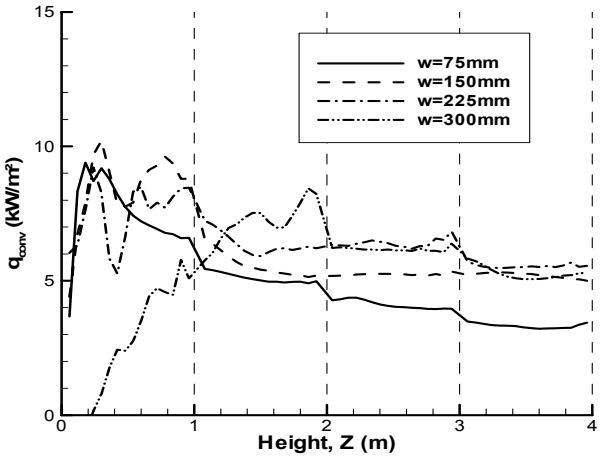

(c) Established fire over the rack

Fig. 12: Evolution of the convective heat flux between the gas and condensed fuel surface as a function of the separation distance

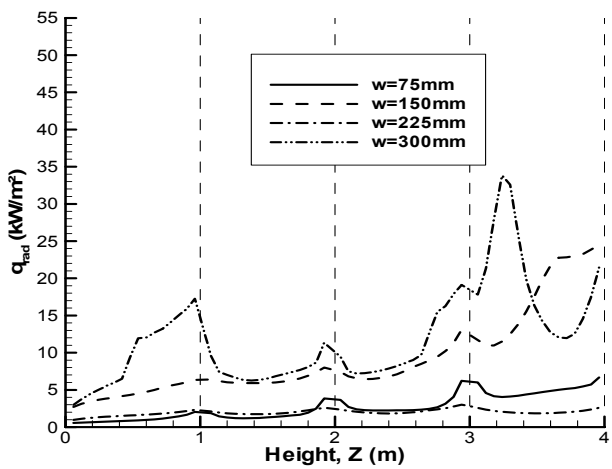

(a) Incipient period

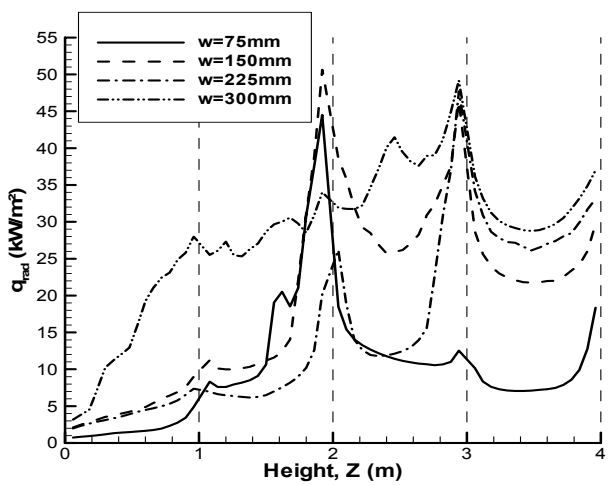

(b) Fire growth period

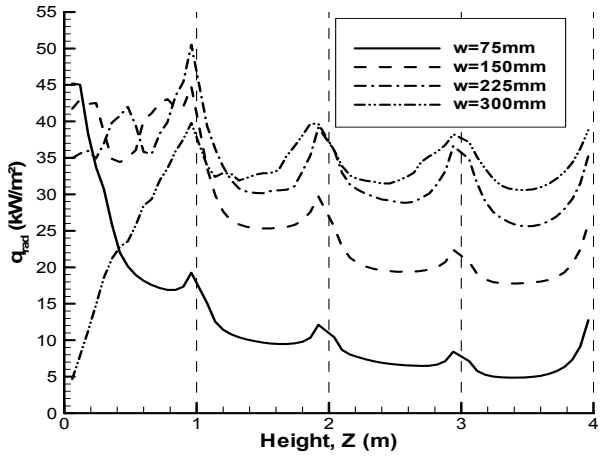

(c) Established fire over the rack

Fig. 13: Evolution of the radiative heat flux from the hotter gas to the condensed fuel surface as a function of the separation distance

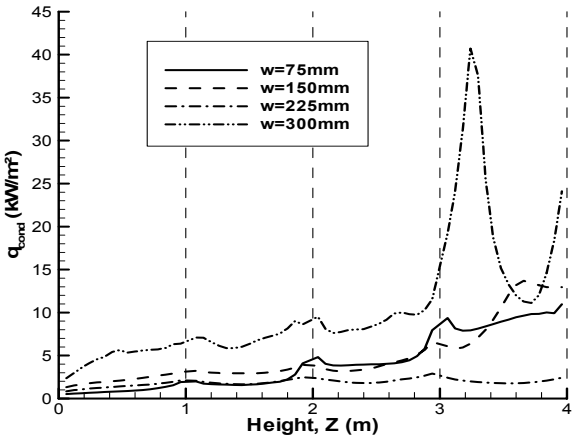

(a) Incipient period

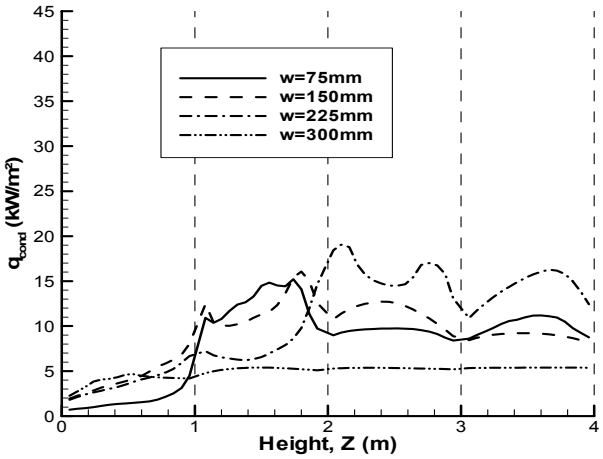

(b) Fire growth period

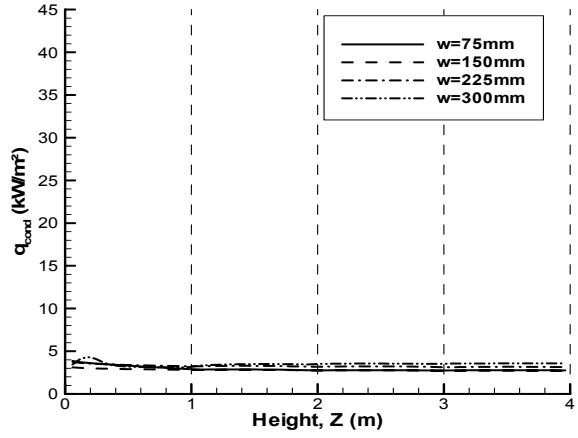

(c) Established fire over the rack

Fig. 14: Evolution of the conduction loss flux in the condensed phase as a function of the separation distance

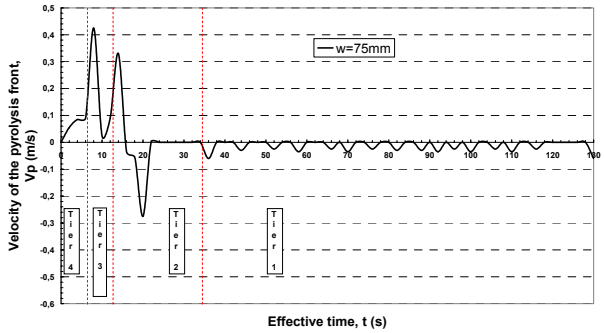

(a) w = 75 mm

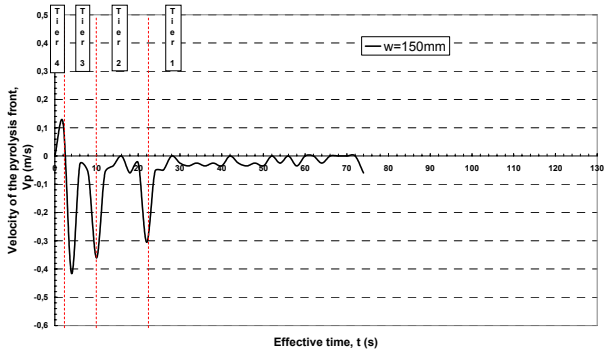

(b) w = 150 mm

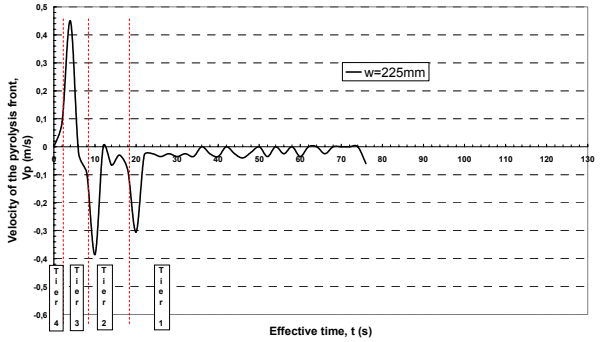

(c) w = 225 mm

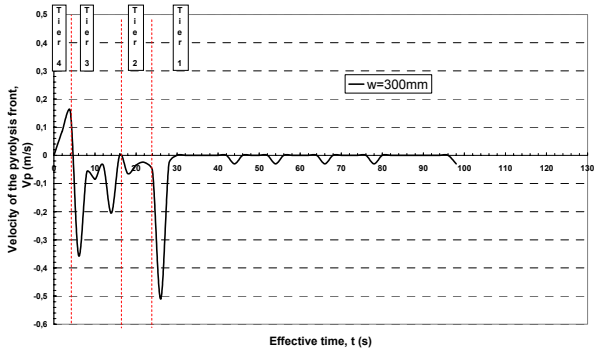

(d) w = 300 mm

Fig. 15: Effect of the ratio, w/h, on the flame spread velocity vs time

The variation of the pyrolysis front, along the same vertical line as indicated in Fig. 11, from z_p to $z_p + \Delta z_p$ vs time interval Δt gives the average flame spread velocity, V_p, as shown in Fig. 15a to d as a function of the separation distance. The overall flame spread process can be divided into two modes, such as the upward (positive value) and downward (negative value) flame spread. Corresponding to the heat flux distribution (Figs. 12 and 13), the ignition occurs first at the high part of the rack storage. For the separation distance of w = 75 mm, the fire spreads upward from the third tier to fourth one with V_p varying from 0.3 to 0.4 ms^{-1}; however, at the level of the second tier, the flame spreads slowly downward towards the rack base. At the level of the fourth tier, the upward flame spread increases first from 0.1 to 0.4 ms^{-1} for an increase of the separation distance from 150 to 225 mm, and later decreases to 0.1 ms^{-1} for w = 300 mm. At the level of the second tier, an increase of the separation distance tends to enhance the downward flame spread velocity up to 0.5 ms^{-1}. It appears that from the second tier, the upward or downward flame spread is in a flapping manner, mainly due to the strongly oscillated reacting flowfield. However, at the level of the first tier, the flame spread velocity is rather weak with a value of 5 cms^{-1}, controlled mainly by the thermal diffusion.

4. CONCLUSION

Numerical study is performed for providing fundamental information about the unsteady behavior of self-sustained solid fuel combustion. Effects of the separation distance between the condensed fuel in rack storage on the flame structure, velocity field and heat transfer is clearly shown. Globally, the predicted results for a rack fire are found in good agreement with the experimental data, and some correlations are developed for determining the flame height in rack storage. For a range (75 – 300 mm) of the separation distance considered here, the spacing of w = 300 mm produces two separated diffusion flames all along the rack, whereas the spacing lower than 300 mm generates a transition flame structure that enhances significantly the flame growth rate. The heat release rate increases first with the spacing, and decreases later once the spacing exceeds a critical value of w = 150 mm. The flame spread in rack storage is mainly due to the strong contribution by radiation, and only for the narrow spacing of w = 75 mm, the convective flux may become a dominant mode of heat transfer. Starting from the second tier, the flame spread over surface of the condensed fuel in rack storage is in a flapping manner. The flame height increases with a decrease of the separation distance, w, due to an increase of the buoyancy effects. Overall, these results can be used to improve the distribution of condensed fuel in rack storage in a warehouse.

It would be highly desirable to relate the flame spread of a condensed fuel to a realistic treatment of the pyrolysis reaction kinetic mechanisms. Moreover, prediction of the heat flux depends strongly on the choice of the soot mass fraction. Future development should relate the soot generation rate to the local oxygen and temperature fields. More research should be also accounting for a dynamic subgrid-scale turbulence model. It would be extremely important to extend predictive capabilities to real warehouse fires in the presence of a large number of potentially flammable racks.

NOMENCLATURE

A	frequency factor
A_m	area of cell face
C_p	specific heat
E	activation energy
f	mixture fraction
g_i	acceleration of gravity
h	total enthalpy or carton height
h_0	distance from the first tier base to ground level
H	total rack height
H_o	heat release rate per unit mass of oxygen consumed
I	radiative intensity
I_m	discretized radiative intensity
Gr	Grashof number
k	thermal conductivity of the condensed fuel
L_f	flame height
$\dot{m}_s$	local burning rate per unit area
n_m	normal direction of the cell face m
p	pressure
p_0	surrounding pressure
Pr_t	turbulent Prandtl number
$\dot{q}_c$	rate of heat release per unit volume
$\dot{q}_{conv}$	convective heat feedback to the pyrolyzing surface
q_r	radiant energy flux
$\dot{q}_{rad}$	flame radiation to the pyrolyzing surface
$\dot{q}_{pyro}$	energy for pyrolyzing fuel
Q	total heat release rate
R	ideal gas constant
Re	Reynolds number
Sc_t	turbulent Schmidt number
S_{ij}	strain rate tensor
T	temperature
T'	temperature fluctuation
u	velocity
u'	velocity fluctuation
w	horizontal separation distance between the condensed fuel

$U_{z,max}$	maximum streamwise velocity at a given height
$U^*_{z,max}$	maximum adimensional streamwise velocity
V	cell volume
W_i	molecular weight of specie, i
x,y,z	streamwise and cross-stream coordinates, respectively
Y_i	mass fraction of the chemical specie, i
Y_{soot}	parameter of soot yield
z_0	virtual source location

Greek Symbols

ε_w	burning surface emissivity
μ_t	turbulent viscosity
ρ	density
κ	total absorption coefficient
$\dot{\omega}_o$	oxygen mass consumption
τ_{ij}	Reynolds stresses
$\delta\Omega^l$	control angle in Finite Volume Method
$\vec{\Omega}$	direction of the radiation propagation

Overhead

-	resolved component
‘	subgrid scale component

Subscripts

s	condensed fuel
g	index of the gas

REFERENCES

1. L.A. Kennedy and O.A. Plumb, “Prediction of buoyancy controlled turbulent wall diffusion flames”, Sixteenth Symposium (International) on Combustion, The Combustion Institute, Pittsburgh, p. 1699 (1977).
2. H. Ahmad and G.H. Faeth, “Fire induced plumes along a vertical wall Part III - The turbulent combusting plume”, National Bureau of Standards Center for Fire Research Grant N°5-9020 (1978).
3. Y. Hasemi, M. Yoshida, N. Yasui and W.J. Parker, “Upward flame spread along a vertical solid for transient local heat release rate”, Proceedings of Fourth International Symposium on Fire Safety Science, p. 385 (1994).
4. L. Orloff, J. De Ris and G.H. Markstein, “Upward turbulent fire spread and burning of fuel surface”, Fifteenth Symposium (International) on Combustion, The Combustion Institute, p. 183 (1978).
5. Z. Yan and G. Holmstedt, “CFD simulation of upward flame spread over fuel surface”, Proceedings of Fifth International Symposium on Fire Safety Science, p. 345 (1997).
6. M.M. Delichatsios, M.K. Mathews and M.A Delichatsios, “An upward fire spread and growth simulation”, Proceedings of Third International Symposium on Fire Safety Science, p. 207 (1991).
7. F. Tamanini and A.M. Moussa, “Experiments on the turbulent burning of vertical parallel walls”, Combustion Science and Technology, Vol. 23, p. 143 (1980).
8. H.Y. Wang, P. Joulain, “Numerical study of the turbulent burning between vertical parallel walls with a fire-induced flow”, Combustion Science and Technology, Vol. 154, p. 119 (2000).
9. G. Heskestad, “Flame heights of fuel arrays with combustion in depth”, Proceedings of Fifth International Symposium on Fire Safety Science, pp. 427-438 (1997).
10. G. Heskestad, “Peak gas velocities and flame heights of buoyancy-controlled turbulent diffusion flames”, Eighteenth Symposium (International) on Combustion, The Combustion Institute, pp. 951-959 (1981).
11. H.Z. You and H.C. Kung, “Strong buoyant plumes of growing rack storage fires”, Twentieth Symposium (International) on Combustion, The Combustion Institute, p. 1547 (1984).
12. H.C. Kung, H.Z. You and R.D. Spaulding, “Ceiling flows of growing rack storage fires”, Twenty-first Symposium (International) on Combustion, The Combustion Institute, p. 121 (1986).
13. H.Z. Yu and P. Stavrianidis, “The transient ceiling flows of growing rack storage fires”, Proceedings of Third International Symposium on Fire Safety Science, p. 197 (1991).
14. H. Ingason, “Effects of fuel spaces on the initial In-rack plume flow”, Seventh International Symposium on Fire Safety Science, p. 235 (2003).
15. K.B. McGrattan, P.F. Glenn and E.F. Jason, Fire Dynamics Simulator, Technical reference guide, NIST Technical Report (2000).
16. W.A. Fiveland, “Discrete ordinates solutions of transport equation for rectangular enclosures”, Journal of Heat Transfer, Vol. 106, pp. 699-706 (1984).
17. M.A. Delichatsios, “Air entrainment into buoyant jet flames and pool fires”. Combustion and Flame, Vol. 70, pp. 33-46 (1987).